Chapter 7

Type-II Superlattice Heterojunction Photodetector with Optoelectronic Characterization and Analytical/ Numerical Simulation

Sanghyun Lee and Kent J. Price

Additional information is available at the end of the chapter

http://dx.doi.org/10.5772/intechopen.71327

Abstract

This chapter focuses on characterization, modeling, and simulation about the type-II superlattices photodetector application. Despite dramatic improvements in type-II superlattices in the past 15 years, challenges still exist in InAs/GaSb and InAs/GaInSb superlattices: The diffusion current, Shockley-Read-Hall (SRH) recombination current, tunneling current, and surface leakage current at elevated temperature. To establish a set of modeling and simulation input parameters, in-depth materials and device characterization at different conditions are carried out for initial materials and device models. Based on input parameters, we will describe the development of analytical and numerical models of InAs/GaSb and InAs/GaInSb type-II superlattice-structured materials and device systems. At the end of this chapter, the fitting of modeled and simulated data will be performed to compare empirical data and modeling results at a set of temperature, which will provide guidance to achieve the higher performance.

Keywords: photodetector, superlattices, type-II, infrared detectors, modeling

1. Introduction

In the last decade, the type-II superlattice has been proposed as a promising candidate for the next generation of IR photodetectors in the long wavelength IR (LWIR) range. The InAs/GaSb and InAs/GaInSb type-II superlattices are considered to be equivalent to HgCdTe with superior cutoff wavelength beyond 15 μm which offers better stability and leverage [1, 2]. Moreover, InAs/GaSb and InAs/GaInSb type-II superlattices provide numerous advantageous optoelectronic properties such as high absorption coefficient, higher effective mass of electrons and holes, slower Auger recombination rate with a proper design of the valence

band structure, a lower dark current, and higher operating temperatures. These make InAs/GaSb and InAs/GaInSb type-II superlattices comparable to established HgCdTe IR photodetectors with the high quantum efficiency [3–6].

The effective band gap of InAs/GaSb and InAs/GaInSb type-II superlattices can be engineered with great flexibility to match mid to far infrared photon energies by selecting appropriate thicknesses for the alternating InAs and GaSb (or GaInSb) layers during crystal growth [3]. Hence there are different performance levels which demonstrate the possibility of multiple band detectors with short wave infrared (SWIR), mid-wave infrared (MWIR), and long wave infrared (LWIR) detectors. In particular, MWIR InAs/GaSb superlattice photodiode application to a focal plane array (FPAs) shows the successful operation at 77 K [7]. The electronic band structure of InAs/GaSb and InAs/GaInSb superlattices enables a spatial separation of holes and electrons localized into different quantum wells. Furthermore, the alternating InAs and GaSb (or GaInSb) layers enable strain in InAs/GaSb and InAs/GaInSb type-II superlattice systems which reduces the Auger recombination rate and therefore, improves the detectivity of the photodetectors [8]. Since the current detector technologies including InAs/GaSb and InAs/GaInSb superlattices require significant cooling to be provided to the detectors, for example, down to 4 K, this implementation makes the photodetector system complicated as a whole which makes it impractical due to the high cost and, most of all, a major hurdle to be overcome before market commercialization. At room temperature, detectors can be used only in active mode with external source due to low sensitivity. Hence, the operation at higher temperatures with high quantum efficiencies remains a major challenge for long wavelength IR range detectors. The major sources that contribute to the dark current of InAs/GaSb and InAs/GaInSb are diffusion current, Shockley-Read-Hall (SRH) recombination current, tunneling current, and surface leakage current.

The goal of this chapter is to develop sustainable analytical and numerical models of device and materials which serve as a set of parameters for modeling and simulation. The established parameters will identify the entitled parameters to achieve maximized device performance. To optimize the performance of InAs/GaSb and InAs/GaInSb superlattices devices, the optoelectronic characterization methods will be carried out to provide basic materials input parameters and device key modeling parameters for the modeling and simulation. Based on established theoretical and empirical models, the baseline device and materials will be set up and provide the guidance for the new design concept to develop higher performance devices at elevated operating temperature.

2. Modeling

One of the major advantages of type-II InAs/GaSb and InAs/GaInSb superlattice systems is the ability to tailor the band gap by changing the thicknesses of InAs and GaSb (or GaInSb) layers. Additionally, the superlattices system provides the ability to hetero-engineer the band structure of the devices. As of now, a number of band gap engineered superlattices architectures, such as W-structure, M-structure for heterostructures (pMp or nBn) and complementary barrier infrared detector have been proposed with the improved performance compared to a homojunction design [9–12].

http://dx.doi.org/10.5772/intechopen.71327

Figure 1 shows the band structure of type-II InAs/GaInSb (also similar to InAs/GaSb) superlattices system grown by MBE on GaSb substrates [13]. The bottom of the conduction band of InAs is below the top of the valence band of GaInSb in a periodic manner. In this periodically alternating InAs and GaInSb layers, this typical band alignment separates the electrons and holes into these two different layers. The effects of coherent strain facilitate compressive stress in GaInSb and tensile stress in InAs layers, which results in splitting the light (LH) and heavy (HH) hole bands. Hence, the phenomena enhance the staggered band alignment. Consequently, the energy gap of the superlattice is formed between the localized hole states (E_{HH1}) in GaInSb and the electron states (E_{C1}) in InAs layers. The energy gap decreases monotonically while increasing the concentration of Indium and this is primarily due to increased strain (larger lattice constant of GaInSb).

The need to accurately predict type-II InAs/GaInSb photodetector performance through modeling and simulations becomes important due to the expensive fabrication cost and complexity of quantum sized materials and devices parameters, and lack of appropriate expertise and skill sets. The traditional choice of theoretical study for electronic transport modeling

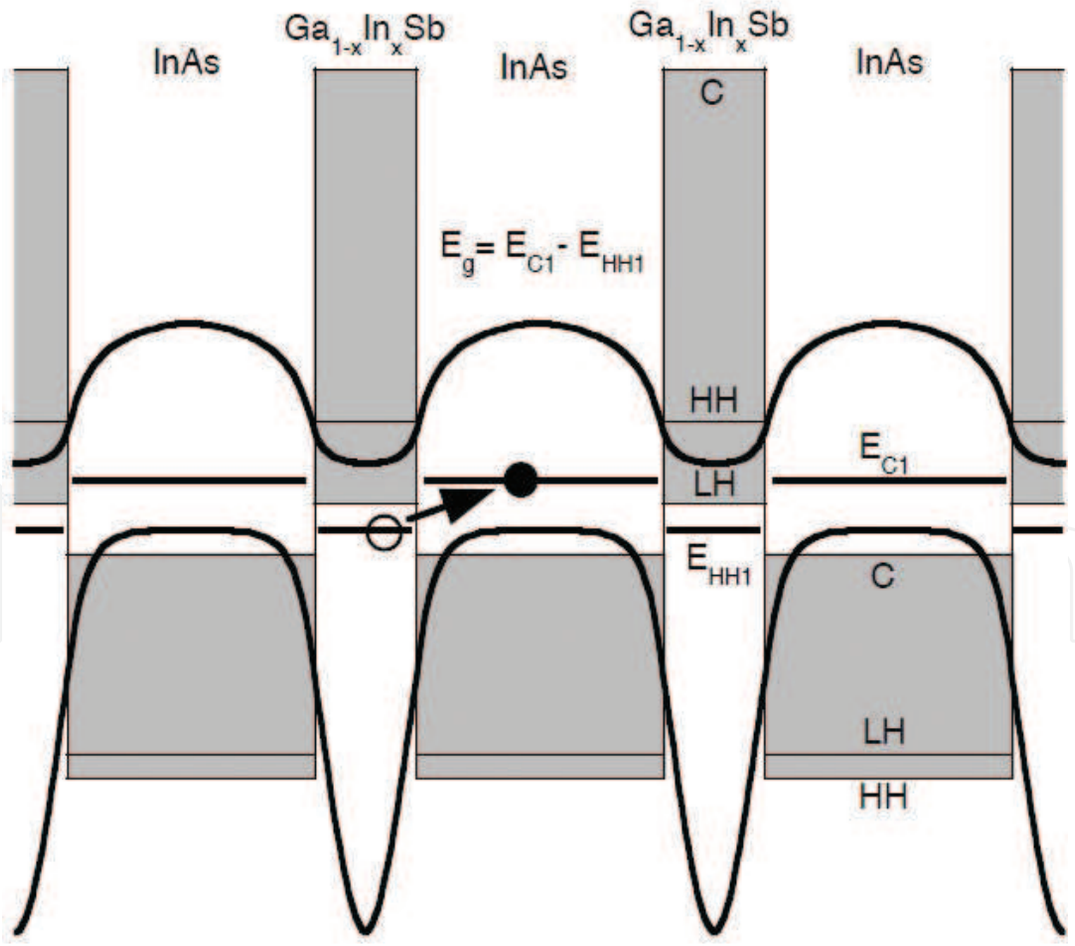

Figure 1. The superlattices energy gap Eg is E_{C1}–E_{HH1}. Energy band structure, electron (E_{C1}) and hole (E_{HH1}) states and corresponding wave functions (Ψ2) in a strained, InAs/GaInSb superlattices grown on GaSb substrate. Shaded parts indicate the forbidden gaps in InAs and GaInSb. The peaks of electron and hole wave functions are situated in different layers [13].

and simulation is governed by two important factors which are the critical spatial dimension of the simulated object (nano-scale alternating film layers) and the physical mechanisms of device operation such as SRH recombination, tunneling, thermionic emission, and temperature effect. The commonly used computational modeling and simulation for transport is described as below. Among these approaches, the drift-diffusion method obtained by using the first moment of the Boltzmann transport equation is the wide-spread methodology in commercially available technology computer aided design simulators (TCAD) such as Synopsys Sentaurus and Silvaco ATLAS. **Figure 2** shows the hierarchical overview of commonly used electronic transport solver for modeling and simulation for the TCAD. These prove an accurate description of carrier transport for the optoelectronic devices. However, the materials and device input parameters need to be precisely calibrated in order to predict the device behavior accordingly.

Over the last decade, there have been similar efforts in a photodetector community such as the k p method [15]. The k p method is used to investigate optical properties of quantum wells, superlattices, heterostructures, and direct-bandgap semiconductors for calculating the electronic structures [14]. The main advantages are to provide,

a. A reasonable compromise in time and model-complexity between simpler approaches such as effective-mass Hamiltonian and tight-binding, ab-initio;

b. Model parameters such as band gap, effective mass, optical matrix elements can be inferred from experiments;

c. An effective way to include strain and spin-orbit interactions;

d. Analytical description of band dispersions near high-symmetry points in Brillouin zone.

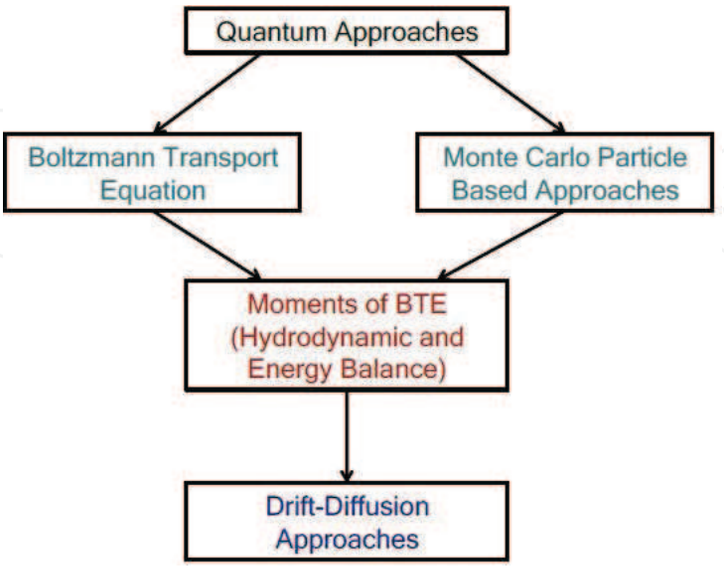

Figure 2. Hierarchical overview of commonly used electronic transport solver for modeling and simulation such as commercial technology computer aided design (TCAD) [14].

For example, Grein et al. [15] described the analytical expression by using this k p method. As a similar effort, Roslan et al. [16] investigated InAs photodiode by using the advanced version of modeling and simulation with 2D Silvaco simulators. To accurately model and simulate, a set of accurate input materials and device parameters should be acquired by optoelectronic characterization such as lifetime, mobility, etc. through a multiple revision processes.

3. Fabrication and characterization methods

The initial step to establish the accurate models is to characterize a set of materials and device input parameters of type-II InAs/GaInSb superlattices, which will be the basis of design parameters for fabricating the device. To achieve their design parameters, there have been a number of approaches to growing InAs/InGaSb superlattices, focusing on the interface layer quality, growth temperature optimization, III–V flux ratios, and substrate effect, etc. [17]. Concurrently, there is a similar amount of efforts to improve GaSb wafers and polishing processes. Although various research groups try to grow the type-II superlattices on Silicon and GaAs substrates, GaSb substrates are able to provide less lattice mismatch related defects than other substrates.

The InAs/GaInSb superlattices samples are typically grown in a molecular beam epitaxy (MBE) system (or MOCVD) equipped with elemental In and Ga solid metal sources and valved As and Sb cracker sources providing $As_2$and Sb_2 [13, 15, 18]. The solid metal sources for In and Ga are SUMO cells designed to reduce spitting and the sources for As and Sb are valved cracker source. The cracker temperature for As and Sb is typically between 800 and 900°C to achieve As_2 and Sb_2 main fluxes over As_4 and Sb_4. The reason for valved cracker design is to ensure the control of As_2 and Sb_2 fluxes at the stage of superlattices growth without further tuning of the cell temperature, which enables the sharp interfaces and the reduction of cross contamination across the layers during switching source flux changes.

The other important processing parameter is the optimization of growth temperature. Based on extensive researches so far, the typical growth temperature is typically between 390 and 430°C to focus on the effects of substrate temperature on superlattices. In this temperature range, superlattices can be optimized to achieve better interface roughness, smoother interfaces at the higher temperature, and residual background carrier concentrations, and so on. To improve further, there have been attempts to utilize short in-situ anneal at higher temperature such as 450°C under a high As flux, which can possibly reduce point defects.

Another important parameter that affects film growth is the film layer growth rate which is very thin compared to other applications. Due to unique thin film growth of superlattices such as a multiple of monolayers (ML), the growth rate is required to be slow to ensure a good quality of the very thin film (<8 nm). Typical growth rates are less than 1 monolayer per second for each layer. With slow growth rates, precision control of the SL period and individual widths has been demonstrated. The samples are grown on n-type (100) GaSb substrates which consisted of a GaSb buffer layer, multiple periods (for example, 40) of superlattices layers, and a GaSb cap layer. The growth is performed with a reflective high-energy diffraction (RHEED) system on a static GaInSb surface [13, 15, 18].

High-resolution x-ray diffraction and atomic force microscopy can be used to confirm the structural quality, composition of the InAs/GaInSb superlattices layers, and the surface morphology. More importantly, the optical properties can be characterized with photoluminescence, absorption spectroscopy, electroluminescence, cathodoluminescence, temperature-dependent I-V, C-V, and deep level transient spectroscopy. Having all the required characterization of input parameters, the initial analytical/numerical modeling and simulation are carried out with MATLAB (k·p in Section 4.1), TCAD (Section 4.2), and Ab-initio methods.

4. Design and modeling of superlattices

The optoelectronic properties of type-II InAs/GaInSb superlattices depend on the energy gap determined by the bottom of the conduction band (CB) of InAs and the bottom of the valence band (VB) of $Ga_{1-x}In_xSb$, where CB maximum of InAs is lower than VB minimum of $Ga_{1-x}In_xSb$. Due to this typical band alignment, the band gap energy of superlattices is smaller than either constituent material, which separates electron (InAs) and holes ($Ga_{1-x}In_xSb$) into the different layers. Moreover, the unique periodic film structure of superlattices allows the separation of heavy and light hole bands by compressive stress ($Ga_{1-x}In_xSb$) and tensile strain (InAs). This staggered band structure of superlattices provides the smaller band gap and spatial separation of electron and hole, which requires spatial indirect transition across the band gap. To achieve good optical transition with sound oscillator strength (hence, good absorption coefficient), the wave functions of the first heavy hole state (E_{HH1}) and the first electron states (E_{C1}) are required to overlap each other. Consequently, the optical absorption of the superlattices is determined by the overlap of the wave function between the localized hole states (E_{C1} in $Ga_{1-x}In_xSb$) and electron states (E_{HH1} in InAs). The overlap of the wave function is strongest in the superlattices design structure due to the enhanced electron and hole wave function overlaps by the repetition of each thin layer. As the thickness of each layer increases, the wave function overlaps rapidly decreases.

In **Figure 3**, the critical thickness by the number of monolayers (ML) is calculated with respect to the Indium composition (x) at 400°C, based on the mechanical equilibrium theory [21]. The composition dependent-strain due to the lattices mismatch is inserted on the top. The critical layer thickness is the maximum strained $Ga_{1-x}In_xSb$ thickness which is dislocation-free. Consequently, the energy gap of superlattices can be modulated between 0 and 300 meV by adjusting the layer width and the alloy composition. In **Figure 4**, the energy gap changes are described as a function of the width of InAs monolayers with respect to Indium concentration at fixed 8 monolayers of GaInSb on the left. Similarly, the variation of energy gap is plotted against the width of GaInSb monolayers at different Indium concentration on the right.

Narrow energy band gap superlattices with good optical properties (in particular, infrared absorption) require designing of thin film layers with the corresponding higher concentration of Indium. This can facilitate the reduction of the layer widths and the energy band gap as well, which enables the application beyond a wavelength of 15 um or very long-wave infrared (VLWIR) detection [18]. The typical indium percentage in the GaInSb layer has not been less

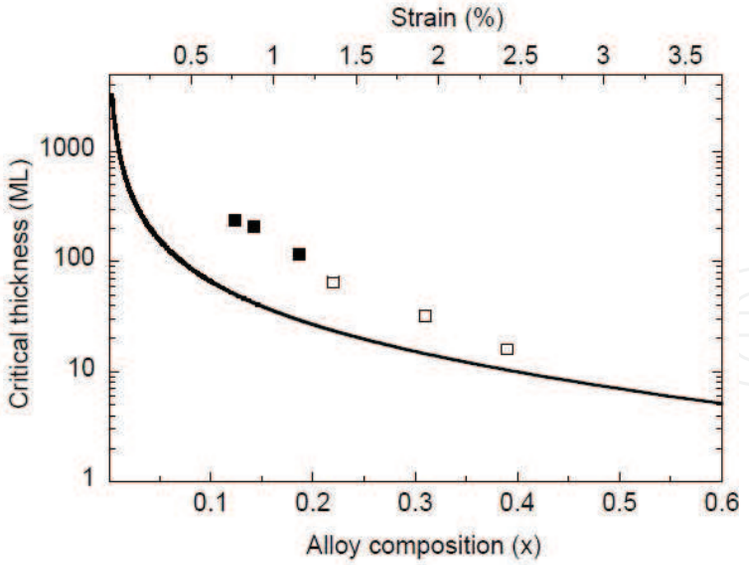

Figure 3. The calculated critical layer thickness in monolayers, ML (solid line) of $Ga_{1-x}In_xSb$ grown on GaSb at 400°C vs. indium concentration, x in $Ga_{1-x}In_xSb$ biaxial compression while InAs biaxial tension which lowers the conduction band and raises the heavy hole band. The experimental data are inserted in the figure (square) [19, 20].

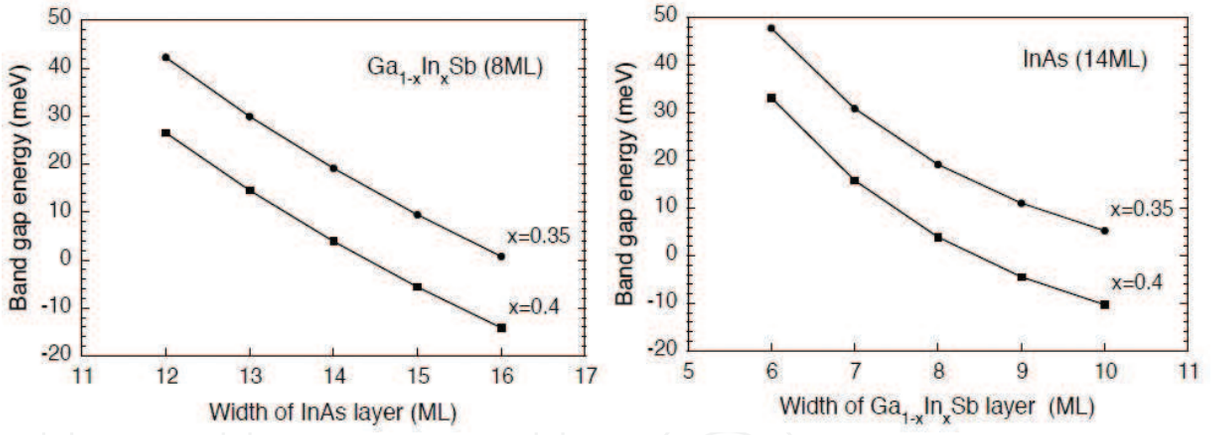

Figure 4. Band gap energy modification in InAs/$Ga_{1-x}In_xSb$ superlattices against the fixed width of $Ga_{1-x}In_xSb$ (left) and InAs (right) monolayers. The film thickness of $Ga_{1-x}In_xSb$ is fixed at 8 monolayers while varying the number of InAs monolayers at different indium concentration, x = 0.35 and 0.40 (left). For 14 monolayers of InAs, the film thickness of $Ga_{1-x}In_xSb$ changes with respect to indium x = 0.35–0.40 (right) [13].

than 30% to avoid the strain imbalance between these superlattices with high Indium concentration and GaSb lattice constant. The absorption coefficient spectra for various Indium concentration in superlattices are demonstrated in **Figure 5**.

4.1. Theoretical modeling: k·p methods

Since there are a number of input parameters that can be modulated to achieve designed superlattices at any given cutoff wavelength, it is imperative to provide a theoretical description

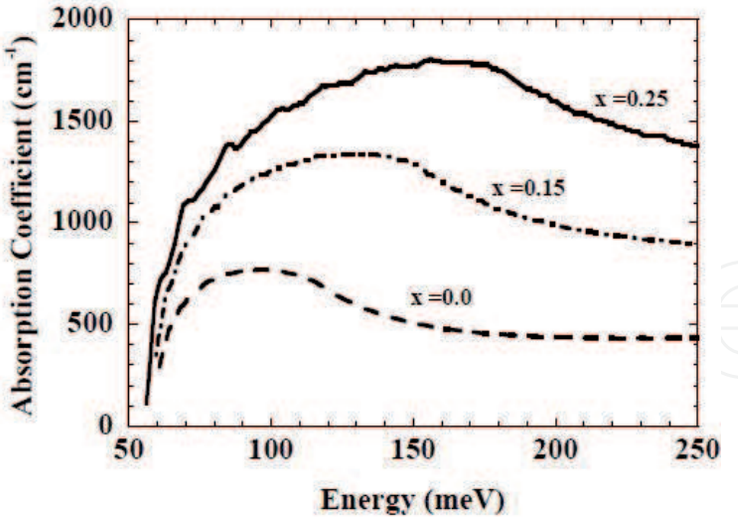

Figure 5. The calculated absorption coefficient spectra for various indium concentration in InAs/$Ga_{1-x}In_xSb$ superlattices design. The three different superlattices are designed to achieve the same narrow band gap with InAs (8.13 nm)/GaSb (2.66 nm), InAs (6.16 nm)/$In_{0.15}Ga_{0.85}Sb$ (2.28 nm), and InAs (5.27 nm)/$In_{0.25}Ga_{0.75}Sb$ (2.04 nm) [17].

by modeling chosen type-II superlattices system with the proper band gap energy, band structure, absorption spectra, and carrier lifetimes. The widely accepted method of the energy band description is the effective-mass approximation, which is also known as superlattice k·p method. It is a popular method for calculating the electronic structure of superlattices because of using a minimal set of parameters to describe and simulate heterostructure electronic properties independent of the number of atoms in the system [17]. The number of energy bands in the k·p Hamiltonian expands from the simple 4-band model to the 14-band model, which provides a continuation in the wave vector k of the energy bands near high-symmetry extremum points in the Brillouin zone such as Γ, X, L points. The simple 4-band model provides the accurate prediction of zone-center transition energies between the conduction and valence band whereas the 14-band model successfully describes the electronic structure throughout the Brillouin zone with the envelope function approximation, which discriminates crystal periodicity from the heterostructure energy envelope [17]. The k·p method is an efficient model to perform the simulation with material level properties up to the device-level properties without atomistic details.

The simulated energy band structure of 14 monolayers of InAs/8 monolayers of $Ga_{0.6}In_{0.4}Sb$ in [001] direction is demonstrated in **Figure 6**. To be consistent with the reported data, a set of material input parameters are taken from the Ref. 22 by using strain-dependent k·p model, including energy gaps, valence band offsets, deformation potentials, lattices constants, and elastic constants.

The superlattice is designed to target the energy gaps between 0 and 50 meV by considering the target layer thickness and alloy compositions. The 14 monolayers of InAs and 8 monolayers of $Ga_{0.6}In_{0.4}Sb$ strained layer superlattice is simulated and compared to the fabricated samples. The MBE grown samples are fed back to the superlattice modeling and design to achieve the target goal of energy gap around 9 meV. The superlattice energy gap is 4 meV,

http://dx.doi.org/10.5772/intechopen.71327

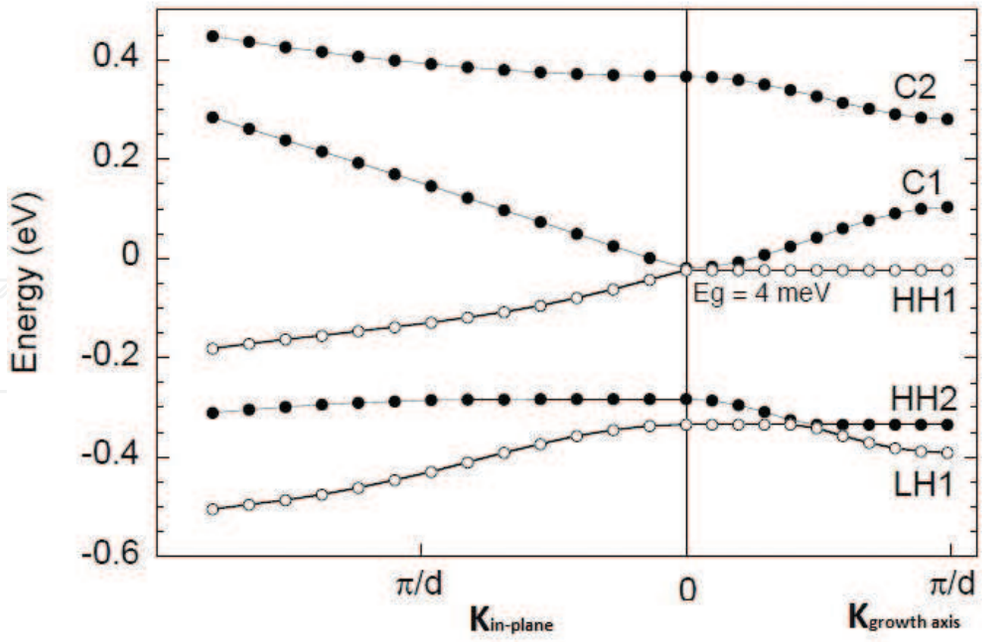

Figure 6. 8-band k·p model, calculating [001] in-plane (left) and growth direction (right) dispersion relations for the strained layer superlattice with 14 monolayers of InAs/8 monolayers of $Ga_{0.6}In_{0.4}Sb$. The period of the superlattices, d is 6.73 nm and the valence band edge of GaInSb happens to be located at zero energy level [13].

which is equivalent to the energy difference between the minimum of the electron energy state (E_{C1}) and the maximum of the heavy hole energy (E_{HH1}) at the zone center. As previously reported [8, 18], a large splitting between heavy hole and light hole energy states suppresses the hole–hole Auger recombination processes when compared to the energy gap along the growth direction (E_{HH1}–E_{LH1} < Eg) and thus, greatly improves the minority carrier lifetime, leading the improved device detectivity (D*) and operating temperature. Based on minimizing the Auger recombination, Grein et al. [15] calculated a strain-balanced VLWIR superlattice structure by using 14-band k·p method (a.k.a. superlattice k·p) to calculate states throughout the zone [8, 15], which is a reformulation of superlattice 14 band k·p method trying to explain Auger recombination and carrier lifetimes of type-II superlattice [15, 23]. In their calculation, a heterostructure restricted basis formalism is used by employing 14 bulk bands non-perturbative calculation [24], which successfully explained the optical properties, carrier recombination rates while incorporating interface bonding effects. The computed superlattice structure of 4.70 nm InAs/2.15 nm $Ga_{0.75}In_{0.25}Sb$ demonstrated a radiative lifetime of 140 ns whereas Auger-1 and Aguer-7 lifetimes were calculated to be more than 1 s, which could provide a theoretical limit of device detectivity of 6.0×10^{14} Johns at 40 K [18]. This long hole–hole Auger lifetime is caused by energy conservation forcing the most probable carriers into regions of lower occupation probability further band edges. **Figure 7** shows the simulated band structure of strained 4.70 nm InAs/2.15 nm $Ga_{0.75}In_{0.25}Sb$ superlattices, indicating the greater strain splitting between the uppermost valence bands, which increases the device detectivity in an order of magnitude. The positions of electrons (open circle) and holes (closed circle) indicates lower occupation probabilities at zone center which lowers the Auger recombination.

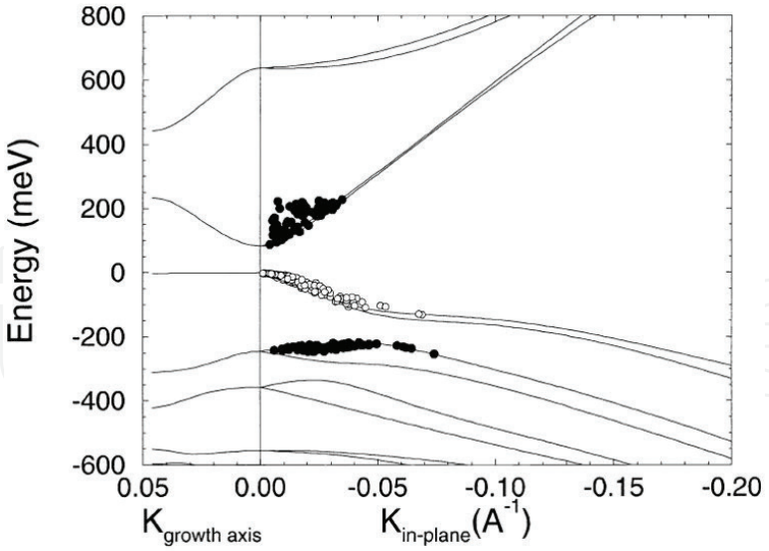

Figure 7. 14-band k·p model, calculating band structure of [001] strained 4.70 nm InAs/2.15 nm $Ga_{0.75}In_{0.25}Sb$ superlattices [001] in-plane (right) and growth direction (left). The positions of electrons (open circle) and holes (closed circle) is superimposed to highlight the lower occupation probabilities and slower Auger recombination at zone center [15].

4.2. Modeling of devices: TCAD

As 8-band k·p envelope function approximation model is used to calculate the band structure, the advantage is the flexibility of the model that can introduce an arbitrary number of layers per superlattice. After the analytical calculation, the resulting band structure can provide input parameters for the electrical device model such as band edge energy and effective masses. Furthermore, absorption coefficient spectra and tunneling coefficient can be modeled and simulated [25, 26]. With type-II InAs/GaSb superlattices, the goal of this section is to provide the TCAD simulation and computation of the electrical performance, in particular, dark current and complete device band structure with various sets of parameters such as composition, doping, and thickness of each layer. As reported in a recent report [27], choosing different period compositions for a given wavelength demonstrates the strong influence of the InAs/GaSb superlattice period thickness and composition on can boost the photodetector performance and material properties [27]. With an asymmetric superlattice period with thicker InAs layer than GaSb layer, the dark current can be reduced by a factor 4 compared to a symmetric superlattice period (equivalent thickness of both films), showing the same cut-off wavelength at 5 um at 77 K.

4.2.1. Modeling of dark current simulation

The main contributor to the dark current at moderate reverse bias is the generation-recombination at low temperature and diffusion current at high temperature. Furthermore, the other main contributors are the trap-assisted tunneling (TAT) via traps and residual dopant, the band-to-band tunneling currents (BTB), and Shockley-Read-Hall (SRH) Generation and Recombination (GR).

The diffusion of thermally generated minority carriers is expressed with a well-known drift-diffusion equation.

$$J_{n,p} = q(n, p)\,\mu_{n,p}\,E \pm q\,D_{n,p}\,\nabla_{n,p}, \tag{1}$$

where J is the current density, q is the charge, μ is the mobility, E is the electric field, D is the diffusion coefficient, and n, p subscripts are to clarify electron and hole components.

SRH recombination rate with trap states (E_t) and intrinsic energy level (E_i) is as below.

$$R_{SRH} = \frac{np - n_i^2}{\tau_p\left[n + n_i\,exp\left(\frac{E_t - E_i}{k\,T_L}\right)\right] + \tau_n\left[n + n_i\,exp\left(\frac{E_i - E_t}{k\,T_L}\right)\right]}, \tag{2}$$

where ni is the intrinsic carrier concentration, τ_n & τ_p are the electron and hole life times, and T_L is the lattice temperature.

The generation–recombination density is the integration along the simulating direction of thickness (W), y.

$$J_{GR} = q\int R_{SRH}\,dy,\ \textit{and integrate upon film thickness, W} \tag{3}$$

Estimating tunneling current is not trivial but if we follow Hurkx [28], the trap-assisted tunneling (TAT) current can be modeled with an additional term, a field effect factor Γ in SRH recombination equation in Eq. (2) [28]. If we modify the lifetime in SRH recombination, the Hurkx model about the field effect enhancement of the trap-assisted current is finally deduced with the net recombination rate (R_{SRH}) as below.

$$R_{SRH} = \frac{pn - n_i^2}{\frac{\tau_p}{1+\Gamma_p}\left[n + n_i\,exp\left(\frac{E_t - E_i}{k\,T_L}\right)\right] + \frac{\tau_n}{1+\Gamma_n}\left[n + n_i\,exp\left(\frac{-E_{Trap}}{k\,T_L}\right)\right]} \tag{4}$$

$$\Gamma_{n,p} = \frac{\Delta E_{n,p}}{k\,T_L}\int_0^1 exp\left(\frac{\Delta E_{n,p}}{k\,T_L}\,u - K_{n,p}\,u^{3/2}\right)du \tag{5}$$

where $\Delta E_{n,p}$ is the energy range where the tunneling of carriers happens and u is the integration term [29, 30]. $K_{n,p}$ is defined as below.

$$K_{n,p} = \frac{4}{3}\frac{\sqrt{2\,m_t\,\Delta E_{n,p}^3}}{q\frac{h}{2\pi}|E|}, \tag{6}$$

where m_t is tunneling mass, E is the electric field, and h is Plank's constant.

As you can see from the above equation, the field effect term considers the phonon-assisted enhancement of the carrier emission from a trap, which is enhanced under accelerated field circumstance. This model combined with GR and TAT current is a set of the simulation and computing in the following sections.

4.2.2. Input parameters for InAs/GaSb superlattices

The basic simulation structure is described in **Figure 8**. The simulated p-i-n device structure of InAs/GaSb superlattices is comprised of p-type GaSb buffer layer (200 nm), p-type 7 monolayers (ML) InAs/4 ML GaSb (1×10^{18} cm^{-3}), intrinsic 7 ML InAs/4 ML GaSb superlattices, n-type 7 ML InAs/4 ML GaSb superlattices (5×10^{17} cm^{-3}). The simulation is performed as a bulk material where the electronic transport inside mini-bands is ignored. To keep the consistency with the recent literature, modeling materials parameters for InAs and GaSb are listed as reported earlier [29–33].

4.3. Modeling and simulation results

Firstly, the band energy diagram is simulated at 77 K with the band gap energy and doping concentration (**Table 1**). As in the recent report [28, 30–33], residual doping is added as mentioned in the previous section. With reference to E_f at 0 eV location, the band diagram is demonstrated in **Figure 9**. The intrinsic doping level is experimentally determined as 2.8×10^{15} cm^{-3} [29].

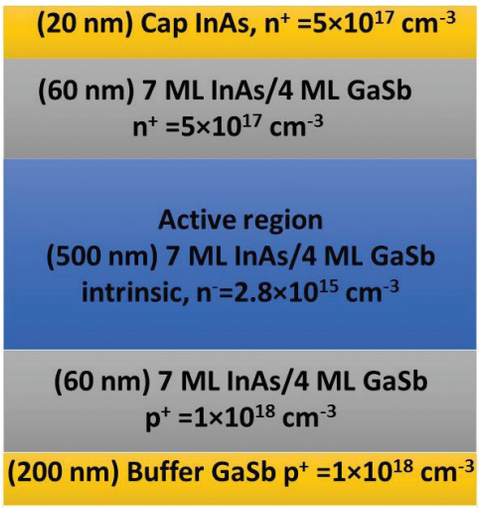

Figure 8. Simulated 7 monolayers (ML) InAs/4 ML GaSb superlattices p-i-n diode structure. Buffer is p-type GaSb, 1×10^{18} cm^{-3} and cap is n-type InAs, 5×10^{17} cm^{-3} for the simulation [29].

Parameter	Symbol	Value	Unit (or multiple of)
Electron effective mass	m_e	0.0254	m_0
Hole effective mass	m_h	0.245	m_0
Electron mobility	μ_e	2.6e4	cm^2/V-s
Hole mobility	μ_P	680	cm^2/V-s
Electron affinity	X	4.73	eV
Permittivity	ϵ	15.34	ϵ_0
Lifetime at 77 K	T	100	ns

Table 1. Input parameters for InAs/GaSb TCAD simulation.

The simulation of dark current curves is carried out at the various temperature from 77 to 237 K in **Figure 10** [29]. On the left hand side (**Figure 10a**), the simulated dark current curves are color-coded whereas empirical data are overlapped on the simulated curves with good matches, in particular, at the lower temperature. On the right hand side (**Figure 10b**), the

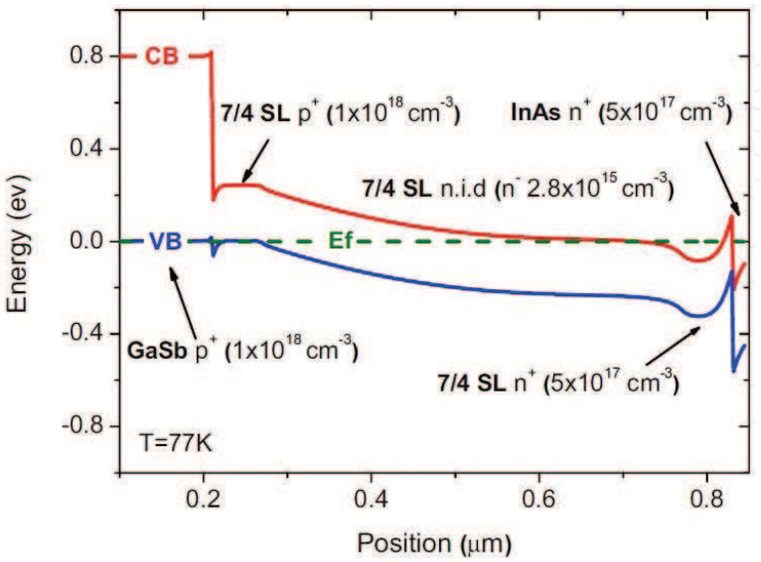

Figure 9. Energy band diagram calculated at 77 K with E_f located at 0 eV. The intrinsic InAs/GaSb superlattices are slightly n-type with 2.8×10^{15} cm^{-3} [29].

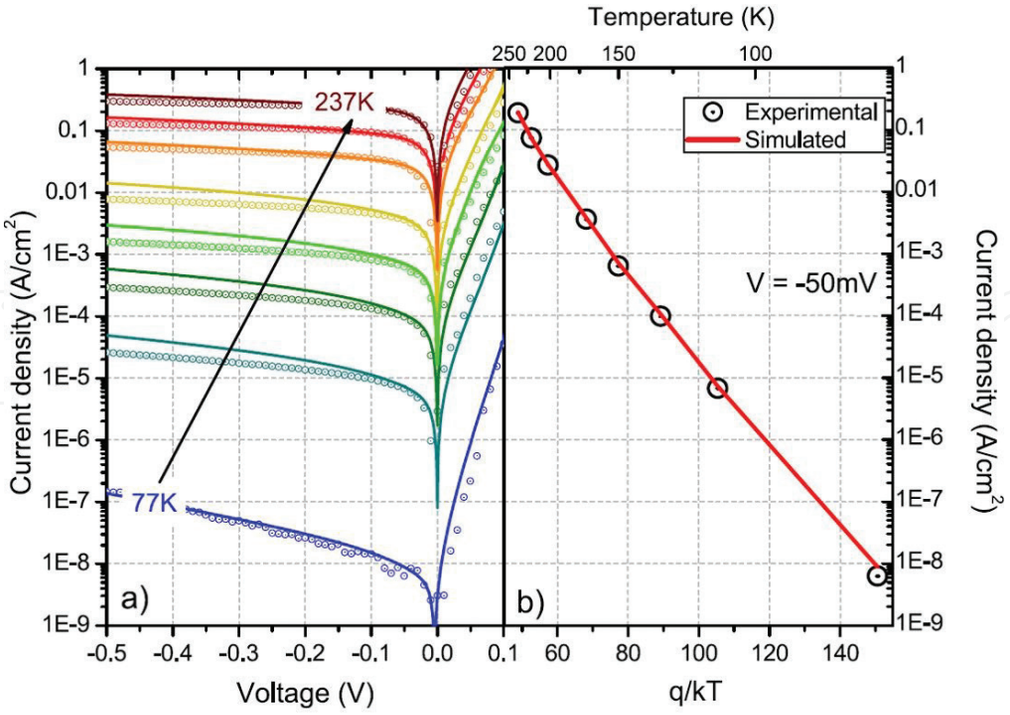

Figure 10. Empirical (open circle) and simulated dark currents (solid line) at different temperatures (a) and Arrhenius plot for the simulated data (solid line) at 50 mV reverse voltage, overlapped with empirical data (open circle) [29].

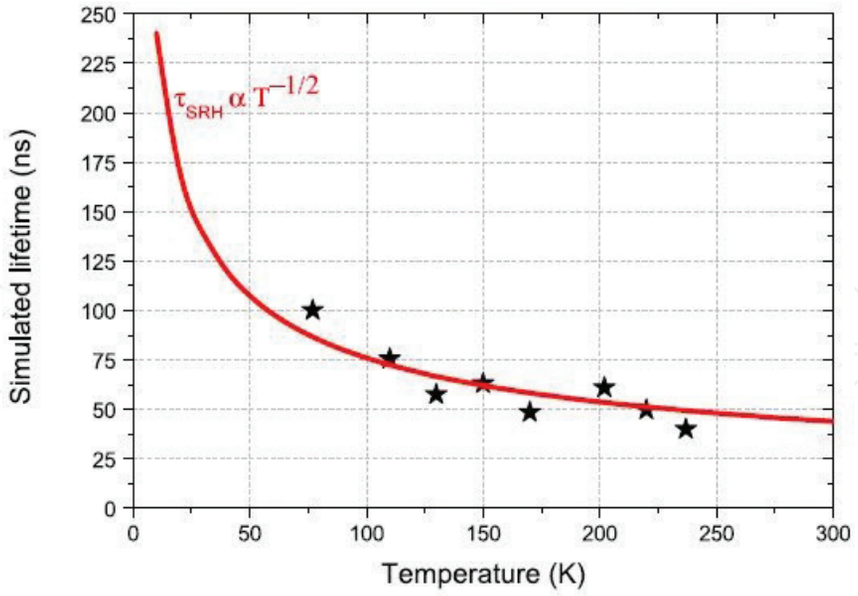

Figure 11. Fitting lifetime curves with power-law of $T^{-0.5}$ as a function temperature (star) [29].

Arrhenius plot of dark current at 50 mV reverse bias, considered to be a turn-on voltage is illustrated which well agrees well empirical data. The fitting of Arrhenius plot consists of the summation of diffusion component and generation-recombination plus trap-assisted tunneling components in the modeling and simulation. **Figure 11** shows the lifetime that is calculated from the simulation as a function of temperature. As you can see in the plot, the lifetime ranges from 50 nm to 100 ns from 77 to 230 K. The fitting of the lifetime is performed with temperature power-law, $T^{-0.5}$ which is the signature of SRH generation-recombination as mentioned by Connelly et al. [34].

5. Summary

In this chapter, we have discussed characterization, modeling, and simulation for the type-II superlattices photodetector application. By modeling with the k·p method, the superlattice band structure is modeled to serve as a set of input parameters for the following TCAD modeling and simulation. The theoretical modeling about Auger lifetime provides the insight about the dramatic reduction of Auger recombination. Furthermore, TCAD simulation and modeling are performed about the band the dark current. The dark current is theoretically characterized under the field effect enhancement of the trap-assisted current as well as SRH recombination and generation. The net recombination rate is finally deduced following a Hurkx model to compute the dark current. Having a tremendous amount of progress in the area of design, growth, and development over the past 15 years, has allowed the modeling and simulation of the type-II superlattices, this will provide new opportunities and guidance to the development of the next generation superlattice photodetector application.

Author details

Sanghyun Lee[1]* and Kent J. Price[2]

*Address all correspondence to: sanghyun.lee@indstate.edu

1 Department of Electronics and Computer Engineering Technology, Indiana State University, Terre Haute, IN, USA

2 Department of Physics, Morehead State University, Morehead, KY, USA

References

[1] Smith DL, Mailhiot C. Proposal for strained type II superlattice infrared detectors. Journal of Applied Physics. 1987;**62**:2545-2548

[2] Rogalski A, Antoszewski J, Faraone L. Third-generation infrared photodetector arrays. Journal of Applied Physics. 2009;**105**:091101

[3] Nguyen BM, Razeghi M, Nathan V, Brown GJ, Nguyen BM, Razeghi M, Nathan V, Brown GJ. Type-II M structure photodiodes: An alternative material design for mid-wave to long wavelength infrared regimes. Proceedings of SPIE. 2007;**6479**:64790S

[4] Kim HS, Plis E, Rodriguez JB, Bishop GD, Sharma YD, Dawson LR, Krishna S, Bundas J, Cook R, Burrows D, Dennis R, Patnaude K, Reisinger A, Sundaram M. Mid-IR focal plane array based on type-II InAs/GaSb strain layer superlattice detector with nBn design. Applied Physics Letters. 2008;**92**:183502P

[5] Delaunay, B. M. Nguyen, D. Hoffman, M. Razeghi. High-performance focal plane array based on InAs-GaSb superlattices with a 10-μm cutoff wavelength. IEEE Journal of Quantum Electronics. 2008;**44**(5):462-467

[6] Grein CH, Flatte ME, Olesberg JT, Anson SA, Zhang L, Boggess TF. Auger recombination in narrow-gap semiconductor superlattices incorporating antimony. Journal of Applied Physics. 2002;**92**:7311

[7] R. Rehm, M. Walther, J. Schmitz, J. Fleissner, J. Ziegler, W. Cabanski, R. Breiter. Dual-colour thermal imaging with InAs/GaSb superlattices in mid-wavelength infrared spectral range. Electronics Lett. 2006;**42**:577-578

[8] Grein CH, Young PM, Flatte ME, Ehrenreich H. Long wavelength InAs/InGaSb infrared detectors: Optimization fo carrier lifetimes. Journal of Applied Physics. 1995;**78**(12): 7143-7152

[9] Kim CS, Canedy CL, Aifer EH, Kim M, Bewley WW, Tischler JG, Larrabee DC, Nolde JA, Warner JH, Vurgaftman I, Jackson EM, Meyer JR. Molecular beam epitaxy growth of antimonide type-II "W" high-power interband cascade lasers and long-wavelength infrared photodiodes. Journal of Vacuum Science and Technology B. 2007;**25**:991

[10] Nguyen B-M, Hoffman D, Delaunay P-Y, Huang E, Razeghi M, Pellegrino J. Band edge tunability of M-structure for heterojunction design in Sb based type II superlattice photodiodes. Applied Physics Letters. 2008;**93**:163502

[11] Nguyen B-M, Bogdanov S, Pour S, Razeghi M. Minority electron unipolar photodetectors based on type II InAs/GaSb/AlSb superlattices for very long wavelength infrared detection. Applied Physics Letters. 2009;**95**:183502

[12] Maimon S, Wicks GW. nBn detector, an infrared detector with reduced dark current and higher operating temperature. Applied Physics Letters. 2006;**89**:2360235

[13] Patrashin M, Hosako I, Akahane K. Type-II InAs/GaInSb superlattices for terahertz range photodetectors. Proceedings of SPIE. 2001;**8188**:81880G-818801

[14] Ganapathi K. Tunneling in Low-Power Device-Design: A Bottom-Up View of Issues, Challenges, and Opportunities. Technical Report No. 2013;UCB/EECS-2013-164

[15] Grein CH, Lau WH, Harbert TL, Flatte ME. Modeling of very long infrared wavelength InAs/GaInSb strained layer Superlattice detectors. Proceedings of SPIE. 2002;**4795**:39-43

[16] Roslan P, Roslan PS, Ker PJ, Ahmad I, Pasupuleti J, Fam PZ. Modeling and simulation of InAs photodiode on electric field profile and dark current characteristics. Applied Physics Letters. 2016 IEEE-ICSE Proc. 2016;**1**:188-191

[17] Brown G. Type-II InAs/GaInSb Superlattices for infrared detection: An overview. Proceedings of SPIE. 2005;**5783**:5783-5783(13), Infrared Technology and Applications XXXI. DOI: 10.1117/12.606621

[18] Haugan H, Olson B, Brown G, Kadlec E, Kim J, Shaner E. Significantly enhanced carrier lifetimes of very long-wave infrared absorbers based on strained-layer InAs/GaInSb superlattices. Optical Engineering. 2017;**56**(9):091604

[19] Kuramochi E, Yoshifumi T. Strain effects in InGaSb/AlGaSb quantum wells grown by molecular beam epitaxy. Journal of Applied Physics. 1995;**77**(11):5706-5711

[20] Nilsen T, Brevik M, Selvig E, Fimland BO. Critical thickness of MBE-grown $Ga_{1-x}In_xSb$ ($x<0.2$) on GaSb. Journal of Crystal Growth. 2009;**311**:1688-1691

[21] Matthew JW, Blakeslee AE. Defects in epitaxial multilayers: I Misfit dislocations. Journal of Crystal Growth. 1974;**27**:118-125

[22] Vurgaftman J, Meyer R, Ram-Mohan LR. Band parameters for III–V compound semiconductors and their alloys. Journal of Applied Physics. 2001;**89**(11):5815-5875

[23] Youngdale ER, Meyer JR, Hoffman CA, Bartoli FJ, Grein CH, Young PM, Ehrenreich H. Auger lifetime enhancement in InAs-$Ga_{1-x}In_xSb$ superlattices. Applied Physics Letters. 1994;**64**:3160

[24] Olesberg JT. Design and Characterization of the Electronic and Optical Properties of Materials for Mid-Infrared Laser Diode Active Regions. [PhD thesis]. Iowa City, Iowa: University of Iowa; 1999

[25] Asplund C, Würtemberg RM, Lantz D, Malm H, Martijn H, Plis E, Gautam N, Krishna S. Performance of mid-wave T2SL detectors with heterojunction barriers. Infrared Physics & Technology. 2013;**59**:22-27

[26] Ashplund C, Wurtemberg RM, Hoglund L. Modeling tools for design of type-II superlattice photodetectors. Infrared Physics & Technology. 2017;**84**:21-27

[27] Taalat R, Rodriguez JB, Delmas M, Christol P. Influence of the period thickness and composition on the electro-optical properties of type-II InAs/GaSb midwave infrared superlattice photodetectors. Journal of Physics D: Applied Physics. 2014;**47**:015101

[28] Hurkx GAM, Degraff HC, Kloosterman WJ, Knuvers MPG. A new analytical diode model including tunneling and avalanche breakdown. IEEE Transactions on Electron Devices. 1992;**39**:2090

[29] M. Delmas, J-B Rodriguez, P. Christol. Electrical modeling of InAs/GaSb superlattice mid-wavelength infrared pin photodiode to analyze experimental dark current characteristics. Journal of Applied Physics. 2014;**116**:113101

[30] Callewaert F, Hoang AM, Razeg M. Generation-recombination and trap-assisted tunnelling in long wavelength infrared minority electron unipolar photodetectors based on InAs/GaSb superlattice. Applied Physics Letters. 2014;**104**:053508

[31] Svensson SP, Donetsky D, Wang D, Hier H, Crowne FJ, Belenky G. Growth of type II strained layer superlattice, bulk InAs an GaSb materials for minority lifetime characterization. Journal of Crystal Growth. 2011;**334**:103-107

[32] Murray LM, Lokovic KS, Olson BV, Yildirim A, Boggess TF, Prineas JP. Effects of growth rate variations on carrier lifetime and interface structure in InAs/GaSb superlattices. Journal of Crystal Growth. 2014;**386**:194

[33] Nguyen BM, Hoffman D, Delaunay PY, Huang E-K, Razeghi M. Very high performance LWIR and VLWIR type-II InAs/GaSb superlattice photodiodes with M-structure barrier. Proceedings of SPIE. 2008;**7082**:708205

[34] Connelly BC, Metcalfe GD, Shen H, Wraback M. Direct minority carrier lifetime measurements and recombination mechanisms in long-wave infrared type II superlattices using time-resolved photoluminescence. Applied Physics Letters. 2010;**97**:251117

IntechOpen